Numerical Simulation of Guided Ultrasonic Waves in Fiber Metal Laminates including Model Reduction Methods

Natalie Rauter[1,*], Andrey Mikhaylenko[1], Nanda Kishore Bellam-Muralidhar[2], Dirk Lorenz[2] and Rolf Lammering[1]

[1] *Helmut-Schmidt-University / University of the Federal Armed Forces Hamburg, Holstenhofweg 85, 22043 Hamburg, Germany, Email: natalie.rauter@hsu-hh.de*

[2] *Technische Universität Braunschweig, Universitätsplatz 2, 38106 Braunschweig, Germany*

Introduction

In aerospace engineering, vehicle construction and also in the design of many load-bearing structures, it is necessary and appropriate to use lightweight materials and material systems and to apply lightweight construction principles. In the aerospace industry, fiber-metal laminates (FMLs) are of great interest because they combine the ductile properties of metal with the high specific stiffness of fiber-reinforced plastics, and because they are suitable for manufacturing thin-walled shell structures. FMLs are built up in layers and usually have a complex cross-section. For this reason, it is almost impossible to detect structural defects such as delaminations by visual inspection, as these hidden defects occur at the interface between different layers. However, since these defects can lead to a catastrophic failure of the structure, it is necessary to have a reliable method for the detection of such defects in thin-walled plates and shells.

Structural health monitoring (SHM) by means of guided ultrasonic waves (GUW)is a suitable technique to detect damage like impact-related delaminations between different layers using the physical phenomena of wave propagation and its interaction with structural defects. Observing the wave propagation and the interaction of the wavefield with damage provides information about the condition of the structure, [1].

In this work, numerical simulations are carried out to analyze the potential of GUW in FML. However, due to the layered structure and the impedance difference between the used materials, a numerical model with a high resolution in space and time results in a high number of degrees of freedom. This limits the usability of the numerical model for inverse algorithms that are often used for damage localization and damage characterization within SHM with GUW. Therefore, this study first develops a 2D numerical model that can be used to simulate the propagation of GUW in FML and its interaction with damage such as delamination. For validation, the numerically obtained displacement field is compared to analytical solutions derived from the equation of motion. In the second part, a model order reduction procedure is developed, which allows the use of the forward model in the context of inverse techniques. Due to the stochastic characteristic of the damage location and the size of the damage, a parametric model order reduction is used.

Analytical framework

The description of wave propagation in a thin-walled isotropic medium was originally described in [2]. The extension for GUW to transversely-isotropic material and composites can be found in [1], [3] and [4]. The analytical treatment, which comprises the solution of the equation of motion with stress-free boundary conditions at the upper and lower surface of the waveguide, reveals the dispersive nature of GUW. The description of the dispersive behavior of the wave propagation can be summarized in dispersion curves, which show the dependence of the phase and group velocities from the excitation frequency. The analytical formulation of the governing equations starts with the balance of momentum

$$div\,\boldsymbol{\sigma} - \rho_0 \ddot{\boldsymbol{u}} = \mathbf{0}\,. \tag{1}$$

Here, $\boldsymbol{\sigma}$ is the stress tensor, $\ddot{\boldsymbol{u}}$ the second derivative of the displacement field $\boldsymbol{u}$ with respect to time, and ρ_0 the density of the waveguide. Implementation of the linearized strain-displacement relation and the generalized Hooke's law leads to the governing differential equations in the displacements $\boldsymbol{u}$, called Lamé-Navier-equations.

The resulting equations are solved for the displacement components u_a using the following approach

$$u_a = A\,p_a e^{i(k_j x_j - \omega t)}\,. \tag{2}$$

Here, A denotes the amplitude, p_a the components of the polarization vector, x_j the spatial coordinates, t the time, ω the angular frequency and k_j the components of the wave number vector. Without generality exclusion, k_j can be defined in such a way that the first component coincides with the observation direction of the wave. This is formulated by

$$k_j = \begin{pmatrix} 1 \\ 0 \\ \alpha \end{pmatrix}\,, \tag{3}$$

where $\alpha = \tan\,\beta$ holds and β is the angle between the resulting wave number vector and the longitudinal direction. Using Equation (3) it is possible to set up and solve the Christoffel equation. As a result, the dispersion curves for a homogenous single layer are obtained. Now, it has to be taken into account, that a multilayer FML

plate is studied within the scope of this work. Therefore, it is necessary to extend this analytical consideration from a single layer to a layered structure. For this purpose, the Global Matrix Method is used here. This technique for the description of the wave propagation in a layered structure is described in detail in [4], [5]. Based on the derived dispersion curves for the investigated plate it is possible to calculate the displacement field of each wave in the plate at any given point in the dispersion diagram. The determined displacement fields are used to validate the finite element model, which is described in the next Section.

Numerical simulation

For the numerical simulation, an FML made of steel and carbon fiber-reinforced plastic (CFRP) is used. The material properties of the individual layers are provided in Table 1. The stacking sequence is chosen symmetrically and is given by $[\text{steel}/0_4/\text{steel}/0_2]_s$ so that the specimen consists of sixteen layers in total. In addition, the steel and CFRP layers have a thickness of $t_{steel} = 0.12\,\text{mm}$ and $t_{CFRP} = 0.125\,\text{mm}$, respectively, which gives a total thickness of the specimen of $t_{plate} = 1.98\,\text{mm}$.

Table 1: Material properties in analytical and numerical calculations

	E_{11}	E_{22}	G_{12}	ν_{12}	ν_{23}	ρ
	$[GPa]$	$[GPa]$	$[GPa]$	$[-]$	$[-]$	$[\frac{kg}{m^3}]$
steel	180	180	69	0.3	0.3	7900
CFRP	127	9	5	0.3	0.37	1580

In this study, the numerical simulation is limited to the two-dimensional case. The overall length of the numerical model is set to 1 m to enable undisturbed wave propagation without boundary reflections. Furthermore, a mode selective excitation is realized by a symmetric displacement at the upper and lower left corners of the model. In addition, symmetry boundary conditions are applied to the left edge. A scheme of the numerical model and the boundary conditions is provided in Figure 1. The excitation points are indicated by red circles. The excitation signal consists of a five-cycle sine-burst at a center frequency of 120 kHz. Hence, only the fundamental S0-mode is generated and observed.

For the discretization second-order Lagrange elements are used. Over the thickness, each layer is discretized with one element. In the direction of the wave propagation, the element size is set to 0.5 mm. Furthermore, a plane strain state is assumed. The numerical simulations are carried out with COMSOL Multiphysics®.

The in- and out-of-plane displacement fields of the S0-mode are presented in Figures 2 and 3. For validation of the numerical results, analytically obtained displacement fields are shown as well. Since the solution of the dispersion relation is an eigenvalue problem the displacement fields are normalized to the respective maximum amplitude. It can be seen that the impedance differences between the different layers lead to a very complex displacement field in the numerical simulation. This result is confirmed by the analytical solution. There are only small deviations between the numerically and analytically obtained displacement fields. The maximum deviation of the in-plane component is 0.18% and of the out-of-plane component 0.4%. It can be concluded that the wave propagation in FML can still be described analytically by the propagation of GUW in thin-walled structures. However, the displacement field across the cross-section is much more complex compared with isotropic material due to the impedance differences between the layers.

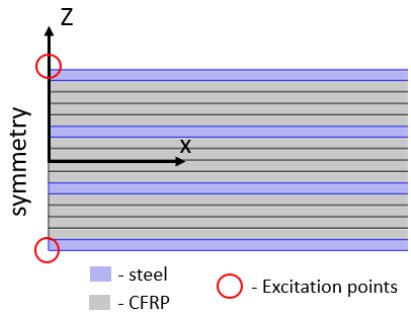

Figure 1: Stacking sequence of the FML specimen

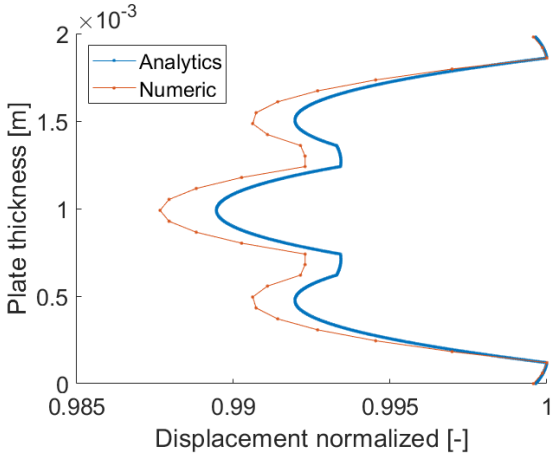

Figure 2: In-plane components of displacement fields: analytic(blue) and numeric(brown) solution for S0-mode.

Parametric model-order reduction

Model-order reduction is an essential technique to overcome the computational challenges in several fields of application. They are employed to produce reduced-order models for the underlying high-dimensional sophisticated systems. These models promise fast simulation without losing the accuracy in their prediction. In this work, the projection-based MOR technique is exploited to generate a ROM. The following second-order undamped structural dynamic ODE is considered for its demonstration.

$$\mathbf{M}\ddot{\mathbf{x}} + \mathbf{K}\mathbf{x} = \mathbf{f} \tag{4}$$

where $\mathbf{M}(\mu), \mathbf{K}(\mu) \in \mathbb{R}^{N\times N}$ are parameterized system global mass and stiffness matrices, $\mathbf{f}(t) \in \mathbb{R}^{N\times m}$ represents load matrix, and $\mathbf{x}(\mu, t) \in \mathbb{R}^{N\times m}$ denotes displacement matrix. $\mu \in \mathcal{P} \subset \mathbb{R}^d$ is the parameter vector describing the system. The approximation of the high-

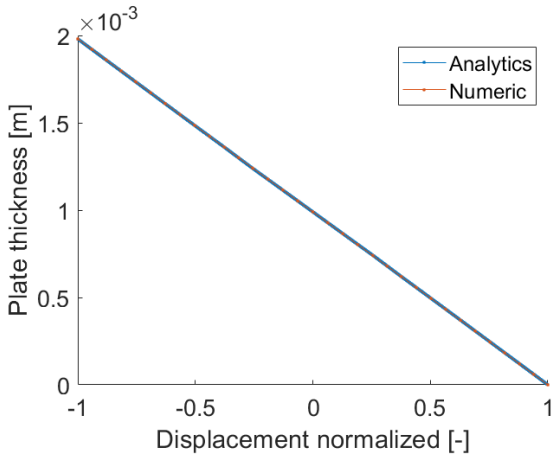

Figure 3: Out-of-plane components of displacement fields: analytic(blue) and numeric(brown) solutions for S0-mode.

dimensional state space $\mathbb{R}^N$ to lower-order $\mathbb{R}^n$ is accomplished by the Galerkin projection method as follows:

$$\mathbf{x} \approx \mathbf{Q}\,\mathbf{x}_r\,, \qquad \ddot{\mathbf{x}} \approx \mathbf{Q}\,\ddot{\mathbf{x}}_r\,. \tag{5}$$

In Equation (5), $\mathbf{Q} \in \mathbb{R}^{N\times n}$ is the projection matrix which is obtained by performing proper orthogonal decomposition (POD) on the snapshot matrix $\mathbf{S}(\mu,t) \in \mathbb{R}^{N\times m}$:

$$\begin{aligned} &\mathbf{S} = [\mathbf{x}_1, \mathbf{x}_2, \ldots, \mathbf{x}_m] && \text{Snapshot matrix} \\ &\mathbf{S} = \mathbf{W}\boldsymbol{\Sigma}\mathbf{V}^T && \text{Singular value decomposition} \end{aligned} \tag{6}$$

$\mathbf{W}(\mu,t) = [\mathbf{q}_1, \mathbf{q}_2, \ldots, \mathbf{q}_m] \in \mathbb{R}^{N\times m}$ is the left-singular matrix with modes, $\boldsymbol{\Sigma} \in \mathbb{R}^{m\times m}$ is a diagonal matrix with singular values $\sigma_1 \geq \sigma_2 \ldots \sigma_m > 0$, and $\mathbf{V}$ is the right singular matrix. The number of mode functions n that capture most of the system's energy was determined by their cumulative energy measure Ξ defined as follows:

$$\Xi = \frac{\sum_{k=1}^{n} \sigma_k}{\sum_{k=1}^{m} \sigma_k}, \qquad n << m. \tag{7}$$

The reduced-order basis (ROB) can then be derived as:

$$\mathbf{Q} = [\mathbf{q}_1, \mathbf{q}_2, \ldots, \mathbf{q}_n] \in \mathbb{R}^{N\times n}. \tag{8}$$

Subsequently, the corresponding ROM can be evaluated in the following manner:

$$\mathbf{Q}^T\mathbf{M}\mathbf{Q}\ddot{\mathbf{x}}_r + \mathbf{Q}^T\mathbf{K}\mathbf{Q}\mathbf{x}_r = \mathbf{Q}^T\mathbf{f} \tag{9}$$

$$\mathbf{M}_r\ddot{\mathbf{x}}_r + \mathbf{K}_r\mathbf{x}_r = \mathbf{f}_r \qquad \text{ROM} \tag{10}$$

with $\mathbf{M}_r, \mathbf{K}_r \in \mathbb{R}^{n\times n}$ and $\mathbf{f}_r \in \mathbb{R}^{n\times m}$. Solving for $\mathbf{x}_r$ and $\ddot{\mathbf{x}}_r$ in (9) and substituting in (5) results in the solution for the full-order system. However, the resulting ROB matrix will be specific to the parameter with which the snapshot matrix is obtained. Employing this ROB matrix to produce ROM for a different parameter will potentially result in a poor approximation and often fails. This triggered a need for parametric model order reduction (PMOR) techniques which yield ROM that is robust to any parameter in the parametric space $\mathcal{P}$. In this research, an adaptive PMOR method along with a surrogate model is utilized to generate global orthogonal modes that approximate the underlying system for any given parameter in $\mathcal{P}$. It seeks to identify the parameter configuration at which the ROM produces the largest error, evaluate the high-fidelity solution for that parameter, and subsequently draw the most influential mode shape of the system using POD. This procedure is repeated in a greedy fashion until a sufficient number of modes are enriched to predict the solution impeccably [6]. As the relative error between the high-dimensional model (HDM) and ROM is not known before solving the HDM, a residual-based *a posteriori* error indicator $\varepsilon(\mu)$ is deployed in this process.

$$\|\varepsilon(\mu)\|_2 = \int_0^{t_{max}} \|\mathbf{f}(t) - \mathbf{f}_h(t)\|dt \tag{11}$$

where, $\mathbf{f}_h$ is the approximation of the load matrix computed by the ROM. The error indicators evaluated in every greedy iteration are called upon to build a multiple linear regression-based surrogate model using which the parameters with a high probability of having the largest error are sampled [6, 7]. This dispenses the effective global modes to produce accurate ROM.

Application of adaptive PMOR

The adaptive PMOR technique based on the POD-greedy approach mentioned in the previous section was applied on GUW propagation in FML with damage. The damage in the FML was introduced in the steel lamina as shown in Figure 4. The damage was modeled as the localized loss of stiffness ($E_{\text{damage}} < E_{\text{steel}}$) in the steel lamina.

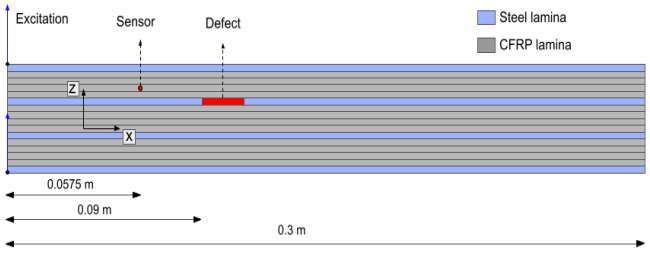

Figure 4: CFRP-Steel laminate with damage

Due to the model-intrusive nature of this PMOR approach, the prominent Newmark's time integration method was utilized to solve the system of equations after extracting the global system matrices from COMSOL®. The training procedure by the presented PMOR method was conducted on $\mu = \{E_{\text{damage}}, x_{\text{damage}}, l_{\text{damage}}\}$ namely Young's modulus, the position of damage on the x-axis, and length of the damage. The parametric space for training was demarcated by $\mu_1 \in [5\times10^6, 5\times10^9]$ Pa, $\mu_2 \in [20, 150]$ mm Pa, and $\mu_3 \in [2, 15]$ mm. The ROM produced by the adaptive POD-greedy method was able to accurately detect the damage present in the FML (see Figure 5).

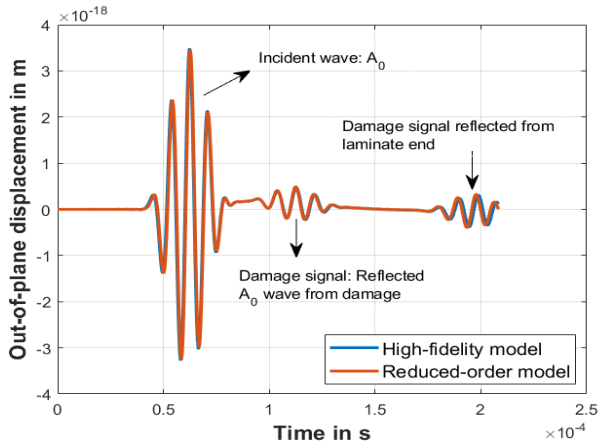

Figure 5: Data reconstruction by the ROM for $\mu = \{4.05\,\text{GPa}, 90\,\text{mm}, 4\,\text{mm}\}$ produced through adaptive POD-greedy approach.

The simulation was performed on a 4-core Intel(R) Core(TM) i7-10510U CPU @ 1.8 GHz processor with 16 GB RAM. The computational efficiency achieved upon PMOR is shown in Table 2. A speedup factor of 33.82 is achieved with the aid of the presented approach.

Table 2: Computation time for HDM and ROM.

Model	Training time	Computational time
HDM	-	66.29 s
ROM	17.6	1.96 s

This significant speedup is very essential when such sophisticated models are used as forward simulators in inverse analysis, often adapted for design optimization, parameter estimation, and uncertainty quantification. As an attempt to test the robustness of the extracted global reduced-order basis, ROMs were generated for two different parameter configurations in $\mathcal{P}$. Their reduced-order solutions (ROS) are illustrated in Figure 6. It is observed that the reflected damage signal was perfectly captured by the ROM and assures its reliability for further analysis. It was required to extract 340 global modes to yield this accuracy.

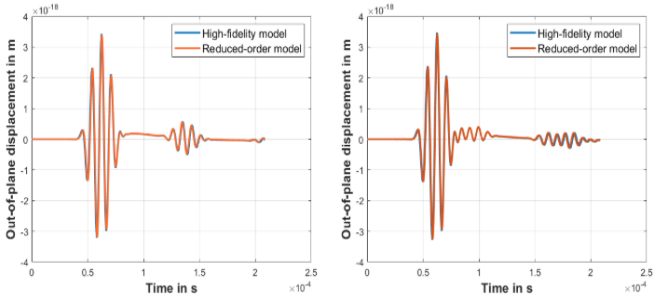

Figure 6: ROS for $\mu = \{1.55\,\text{GPa}, 50\,\text{mm}, 2\,\text{mm}\}$ (left) and $\mu = \{3.55\,\text{GPa}, 70\,\text{mm}, 11\,\text{mm}\}$ (right) evaluated by adaptive PMOR method.

Conclusions

This work shows two aspects to be considered in the numerical analysis of GUW in FML. First, the layered structure of the waveguide leads to complex displacement fields, which have to be considered in the three-dimensional structural analysis. On the other hand, it has been shown that model reduction techniques can be successfully used in the analysis of wave propagation, which is highly beneficial in solving inverse problems for damage localization.

References

[1] Lammering, R., Gabbert, U., Sinapius, M., Schuster, T., Wierach, P. (Eds.): Lamb-Wave Based Structural Health Monitoring in Polymer Composites. Springer International Publishing, 2018

[2] Lamb, H.: On the Vibrations of an Elastic Sphere. Proceedings of the London Mathematical Society. s1-13 (1): 189-212, doi:10.1112/plms/s1-13.1.189, 1881

[3] Rittmeier, L., Losch, T., Sinapius, M., Lammering, R.: Investigation on the influence of material interfaces and impedance changes on the propagation of guided waves in laminated steel layers. Procedia Manufacturing, **24**, 196-202, 2018

[4] Vu, N.: Zur Wellenausbreitung in geschichteten Faserverbundstrukturen unter Verwendung nichtlinearer Stoffgesetze. PhD Thesis, Institute of Mechanics, Helmut Schmidt University Hamburg, 2020

[5] Nandyala, A. R., Darpe, A. K., Singh, S. P.: Effective stiffness matrix method for predicting the dispersion curves in general anisotropic composites. Springer-Verlag GmbH Germany, 2019

[6] Paul-Dubois-Taine, A., Amsallem, D.: An adaptive and efficient greedy procedure for the optimal training of parametric reduced-order models. International Journal for Numerical Methods in Engineering 102.5, 1262-1292, 2015

[7] Jones, D. R.: A taxonomy of global optimization methods based on response surfaces. Journal of Global Optimization 21.4: 345-383, 2001